Pergamon

Int. J. Heat Mass Transfer. Vol. 37, Suppl. 1, pp. 433–445, 1994

0017-9310/94 $6.00 + 0.00

0017-9310(93)E0074-Q

Plate fins with variable thickness and height for air-cooled electronic modules

MIHAELA MOREGA* and ADRIAN BEJAN†

*Department of Electrical Engineering, Polytechnic University of Bucharest, Bucharest 77206, Romania and †Department of Mechanical Engineering and Materials Science, Duke University, Durham, NC 27708-0300, U.S.A.

Abstract—This paper shows that the hot spot temperature of an electronic module with finned air heat sink can be reduced by allowing the fin thickness and height to increase in the flow direction x. The hot spot temperature decreases by about 15% if the thickness of a plate fin with constant height increases as $x^{0.42}$. The decrease is approximately 30% if the height of a constant-thickness plate fin increases as x, i.e. if the fin shape is almost like a triangle when viewed from the side. In addition to lowering the hot spot temperature, the fin thickness and height variations recommended by this study lead to considerably more uniform temperature distributions on the module surface on which the fins are installed.

1. INTRODUCTION

IN THIS paper we explore two ways in which the geometry of finned electronic packages can be optimized so that the thermal contact between the package and the coolant (forced air) is maximized. We consider varying in the flow direction the thickness and the height of the plate fins. The augmentation of air cooling is recognized as an important task in electronics packaging, and promises to gain in importance in the foreseeable future. The reason is that the use of forced air is the most accessible and simplest method of cooling electronics, particularly in instruments and personal computers [1]. These systems must be effective (i.e. functional) *and* robust [2] so that they can operate safely in diverse environments, some of which are hostile (e.g. contaminated air, high temperature and humidity, noise, vibrations). Reviews of air cooling advances [3] and extended surface research [4, 5] do not indicate that the augmentation methods proposed in this paper have been studied before.

The importance of the air cooling augmentation problem is stressed further by the push toward package designs with higher power densities. This trend leads to higher temperatures and higher temperature gradients, which threaten the operation of the electronics. In addition, they lead to differential thermal expansion at the interface between the package and its substrate, and the resulting thermal stresses threaten the integrity of the assembly. To minimize the temperature of the hot spots, and to distribute the temperature as uniformly as possible through the package, is a central objective in the thermal design of electronics. This objective calls for more realistic models, more rigorous analyses, and a more precise fine-tuning of the optimal thermal design.

If we look at a relatively simple example of an electronic package cooled with forced air (e.g. Fig. 1, top), we are struck by the main challenge that confronts the thermal designer: the package is a 'complicated' thermal system. The complications are due not only to the many geometric features (shapes, sizes) that characterize the heat sink and the package, but also to the fact that the conduction through the solid parts is coupled intimately to the flow of the coolant. The flow and its cooling capability change as the designer modifies the geometry of the solid parts.

Because of this coupling and the designer's need to compare many competing configurations, a rigorous way to proceed is by modelling the flow and solid-body conduction as a whole. We illustrate the numerical implementation of this complete (conjugate conduction and convection) model in the last segment of this paper (Section 5). One limitation of this approach is that the flow must be computed every time that the designer makes a change in the geometry. This leads to a numerical design tool that is relatively inflexible and costly.

This is why in the opening part of the paper we try a simpler and more flexible model, which begins with making some assumptions about the local thermal coupling between the air flow and conduction through each fin (e.g. equation (6)). This simple model is then used for the purpose of identifying the degrees of freedom (dimensionless groups) that control the design, and the ways in which these groups can be selected so that the package–coolant thermal contact is improved. Finally, in Section 5 the design trends recommended by the simple model are pursued further by using the complete model in which the flow and solid-body conduction are computed together for a given geometric configuration.

NOMENCLATURE

a	plate sharpness parameter, equation (17)
b	crest inclination parameter, equation (7)
Bi	Biot number, equation (1)
C	constant, equation (8)
D	plate-to-plate spacing, Fig. 1
d	domain dimension, Fig. 6
h	heat transfer coefficient, equation (6)
h_l	h value at $x = L$
$\bar{h}$	order of magnitude of h
H	plate height, Fig. 1
$\bar{H}$	height averaged from $x = 0$ to L
$\tilde{H}$	dimensionless average height, equation (16)
k	thermal conductivity of fin material
k_a	thermal conductivity of air
l, m	domain dimensions, Fig. 6
L	plate length, Fig. 1
n	number of plates
n_c	direction normal to the crest
p	pressure
P	dimensionless pressure, equation (26)
Pe_L	Peclet number, $U_\infty L/\alpha$
q_1	heat transfer removed through one fin
q'	heat transfer rate of one fin, per unit length, q_1/L
q''	heat flux generated by the package
Re_L	Reynolds number, $U_\infty L/\nu$
t	plate thickness
$\bar{t}$	average plate thickness, equation (9)
T	plate temperature
$\tilde{T}$	dimensionless temperature, equation (29)
T_∞	free stream temperature
u, v, w	velocity components
U, V, W	dimensionless velocity components, equation (25)
U_∞	free stream velocity
x, y	Cartesian coordinates, Fig. 1
x, y, z	Cartesian coordinates, Fig. 6
X, Y, Z	dimensionless coordinates, equation (25).

Greek symbols

α	fluid thermal diffusivity
θ	dimensionless excess temperature, equation (11)
θ_{hot}	hot spot excess temperature, equation (18)
ν	kinematic viscosity
ξ, η	dimensionless coordinates, equation (10)
ρ	fluid density
τ	dimensionless plate thickness, equation (11).

Subscripts

$(\ )_{min}$	minimum
$(\ )_{opt}$	optimum.

2. PLATE FIN WITH TWO-DIMENSIONAL CONDUCTION

The development of the fin model used in the present study can seen by reading Fig. 1 from top to bottom. Nakayama *et al.* [6] showed that the heat transfer rate removed from a finned package (Fig. 1, top) reaches a maximum when the air cooled heat sink consists of a certain number (n) of plate fins. Specifically, for a square package ($L \times L$) they reported that $n_{opt} \cong 9$, 10 and 11 when $U_\infty L/\nu = 2000$, 5000 and, respectively, 10000. If the heat transfer through the unfinned portions of the $L \times L$ surface is neglected, the heat transfer rate removed through a single fin is $q_1 = q''L^2/n$, where q'' is the heat flux generated by the package. It is assumed that q'' is generated uniformly over the $L \times L$ area.

Nakayama *et al.*'s [6] optimal number of plate fins is related to the problem of finding the optimal plate-to-plate spacing D_{opt} in a stack of parallel heat generating plates cooled by forced convection. Bejan and Sciubba [7] determined the optimal spacing analytically by assuming that the pressure difference across the stack of parallel plates (ΔP) is known. It is easy to show that by using the pressure difference scale $\Delta P \sim (1/2)\rho U_\infty^2$, Bejan and Sciubba's [7] formula reproduces the optimal numbers of plate fins determined by Nakayama *et al.* [6].

The two studies mentioned above are relevant to the development of the present model for a very important reason. As was shown analytically in Bejan and Sciubba [7], the plate-to-plate spacing is optimal when the boundary layers are thinner than the plate-to-plate spacing, such that they meet only at the exit from the plate-to-plate channel. This means that the heat transfer to the air stream takes place across laminar forced convection boundary layers. It means also that for the purpose of optimizing the design of the heat sink we may focus on a single fin with laminar boundary layers on both sides. The heat transfer input to the single fin is distributed uniformly along the base of the fin, $q' = q_1/L$, constant.

It is important to stress that by focusing on the optimization of a single plate fin we are assuming that the heat sink (i.e. the stack of fins) has already been optimized with respect to selecting the proper number of fins, n_{opt}, or fin-to-fin spacing, D_{opt}.

The model of the plate fin is shown in the lower part of Fig. 1. In accordance with the classical treatment of one-dimensional fins, we assume that the temperature variation across the plate (in the z direction) is negligible in comparison with the temperature changes

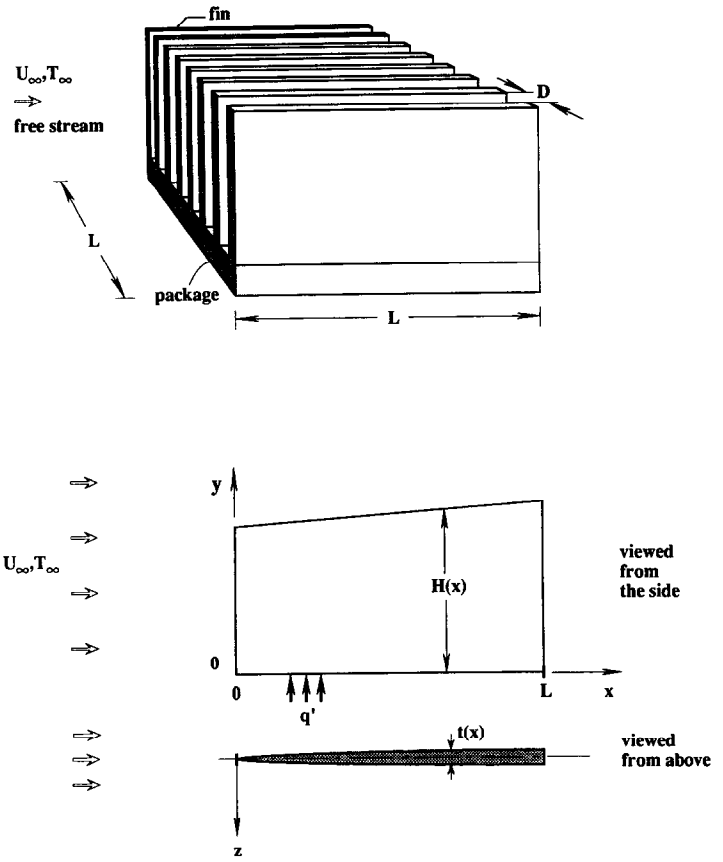

FIG. 1. Forced convection-cooled electronic package with plate-fin heat sink (top), and two-dimensional conduction model for a single plate fin (bottom).

experienced in the x and y direction. This approximation is valid when the Biot number is small (e.g. Bejan [8], pp. 64–65),

$$Bi = \frac{\bar{h}\bar{t}}{k} \ll 1. \tag{1}$$

The plate temperature $T(x,y)$ can be found by solving the fin equation for two-dimensional (x,y) conduction heat transfer,

$$\frac{\partial}{\partial x}\left(kt\frac{\partial T}{\partial x}\right)+\frac{\partial}{\partial y}\left(kt\frac{\partial T}{\partial y}\right)-2h(T-T_\infty)=0 \tag{2}$$

subject to the boundary conditions

$$\frac{\partial T}{\partial y} = -\frac{q'}{kt} \quad \text{at} \quad y = 0 \tag{3}$$

$$\frac{\partial T}{\partial n_c} = 0 \quad \text{at} \quad y = H(x) \tag{4}$$

$$\frac{\partial T}{\partial x} = 0 \quad \text{at} \quad x = 0, L. \tag{5}$$

Equations (4), (5) represent the assumption that the plate is sufficiently thin ($\bar{t} \ll H$) so that the heat transfer through the exposed edges is negligible in comparison with the heat input along the base. Equation (4) is the homogeneous Neumann boundary condition applied on the inclined crest of the plate, where n_c is the direction normal to the crest. The zero-flux condition at the leading edge $x = 0$, equation (5), could be replaced by the Dirichlet condition $T = T_\infty$, because the leading edge assumes the temperature of the free stream. Numerical tests showed that these two conditions, $\partial T/\partial x = 0$ and $T = T_\infty$ at $x = 0$, lead to the same results. The numerical results reported in this paper were obtained using $T = T_\infty$ on the leading edge.

The assumption that the plate has a thin frontal cross-section as it is approached by the fluid means that the flow is oriented mainly in the x direction along the lateral surfaces of the plate. The local heat transfer coefficient h between a point (x,y) on the plate surface and the surrounding free-stream fluid (T_∞) decreases in the x direction, because the boundary layer becomes thicker. The scale analysis of the laminar boundary layer sandwiched between two different temperature scales (T and T_∞, with unspecified distribution of T vs x) showed that h decreases as $x^{-1/2}$ (Bejan [9], p. 38). In this paper we recognize this trend by writing

$$h(x) = h_L\left(\frac{x}{L}\right)^{-1/2} \tag{6}$$

in which h_L is the value of h at the trailing edge. We will use h_L as the representative order of magnitude of h. Note further that equation (6) agrees with the classical h formulas known for the extreme models of the wall with uniform flux and wall with uniform temperature. The present plate fin model falls between these two extremes, most likely very near the uniform flux description (i.e. $h(T-T_\infty) = \text{constant}$ vs x) because of the uniform heat input specified along the base. Finally, note that the h_L scale is relatively insensitive to the manner in which the surface temperature T varies with x: the ratio between the extreme h_L values of the uniform-flux wall and the isothermal wall is $0.453/0.332 = 1.36$.

The geometry of the plate fin was allowed to vary in two ways. The crest of the fin could be inclined relative to the base,

$$H(x) = \bar{H}\left[1 + b\left(\frac{x}{L} - \frac{1}{2}\right)\right] \tag{7}$$

such that the average height $\bar{H}$ remained unchanged. The plate could be sharpened like a knife, the degree of sharpness depending on the exponent a in the plate thickness distribution

$$t(x) = C\left(\frac{x}{L}\right)^a. \tag{8}$$

The volume of the plate fin was fixed,

$$\int_{x=0}^{L}\int_{y=0}^{H(x)} t\,\mathrm{d}y\,\mathrm{d}x = \bar{t}\bar{H}L. \tag{9}$$

The constant C factor that satisfies the volume constraint can be determined by combining equations (8) and (9).

The model constructed between equations (2) and (9) was put in dimensionless form by introducing the variables

$$\xi = \frac{x}{L}, \quad \eta = \frac{y}{(k\bar{t}/h_L)^{1/2}} \tag{10}$$

$$\theta(\xi,\eta) = \frac{T-T_\infty}{q''/(k\bar{t}h_L)^{1/2}}, \quad \tau(\xi,\eta) = \frac{t}{\bar{t}}. \tag{11}$$

The dimensionless equations that replace equations (2)–(5) are

$$\left(\frac{\bar{H}/L}{\tilde{H}}\right)^2 \frac{\partial}{\partial\xi}\left(\tau\frac{\partial\theta}{\partial\xi}\right) + \frac{\partial}{\partial\eta}\left(\tau\frac{\partial\theta}{\partial\eta}\right) - 2\xi^{-1/2}\theta = 0 \tag{12}$$

$$\left(\frac{\partial\theta}{\partial\eta}\right)_{\eta=0} = -\frac{1}{\tau(\xi,0)}, \tag{13}$$

$$\left(\frac{\partial\theta}{\partial\eta}\right)_{\eta=\tilde{H}[1+b(\xi-1/2)]} = 0 \tag{14}$$

$$\theta_{\xi=0} = 0 \quad \text{and} \quad \left(\frac{\partial\theta}{\partial\xi}\right)_{\xi=1} = 0, \tag{15}$$

where

$$\tilde{H} = \frac{\bar{H}}{(k\bar{t}/h_L)^{1/2}}. \tag{16}$$

Worth noting in the dimensionless definition of the average height $\tilde{H}$ is the use of the length scale of conduction penetration in the y direction along the fin, $(k\bar{t}/h_L)^{1/2}$. This means that when $\tilde{H}$ is much smaller than 1 the plate fin is nearly isothermal in the y direction, $\theta(\xi,\eta) \cong \theta(\xi)$. On the other hand, when $\tilde{H}$ is greater than 1, the temperature of the crest of the fin approaches the fluid temperature.

The model presented above shows that the plate fin design is represented by four dimensionless numbers that account for the following features:

a, sharpness of the plate cross-section at y = constant

b, slope of the crest

$\tilde{H}$, inverse of the conduction penetration length in the y direction

$\bar{H}/L$, plate aspect ratio.

The first two numbers govern the shape of the fin, while the last two are fixed when the overall dimensions, fin material and fluid flow are specified. The effect of these numbers was investigated systematically, and is described in the next two sections. The objective is to identify the shapes that lower the temperature of the hot spot that occurs along the base of the fin (i.e. on the package, Fig. 1).

3. PLATE FIN WITH VARIABLE THICKNESS AND UNIFORM HEIGHT

Consider first the class of designs in which the crest of the plate fin is always aligned with the base plane, $b = 0$. In such cases, the volume constraint (9) dictates the following dimensionless expression for the variable thickness,

$$\tau(\xi) = (a+1)\xi^a \tag{17}$$

such that $a = 0$ represents the plate with uniform thickness, and $a = 1$ the sharp-edged plate (i.e. triangular shape when viewed from above).

The plate temperature distribution $\theta(\xi,\eta)$ was determined numerically by solving equations (12)–(15) using finite differences and successive overrelaxation [10]. The chosen variable thickness function, equation (17), creates some numerical difficulties when it is combined with the boundary condition (13). The finite difference method requires that the base plate temperature be expressed as

$$\theta(\xi,0) = \theta(\xi,0+\Delta\eta) + \frac{\Delta\eta}{(a+1)\xi^a}, \tag{18}$$

where $\Delta\eta$ is the grid spacing in the η direction. It is clear that $\theta(\xi,0)$ has a discontinuity close to $\xi = 0$.

Table 1. Accuracy test for the case $a = 0.4$, $b = 0$, $\tilde{H} = 2$, $\tilde{H}/L = 1/3$ (overrelaxation coefficient = 1.95)

Grid	ε	Analytically computed integral (19)	Numerically computed integral (19)	Relative error	Number of iterations	Hot spot temperature (θ_{hot})
30×30	1/29	−1.9024	−1.9047	-1.21×10^{-3}	77	0.6188
40×40	1/39	−1.9803	−1.9823	-9.8×10^{-4}	85	0.6116
50×50	1/49	−2.0316	−2.0333	-8.36×10^{-4}	120	0.6074
60×60	1/59	−2.0684	−2.0699	-7.37×10^{-4}	158	0.6047
102×102	2/101	−2.0923	−2.0929	-3×10^{-4}	350	0.5989

The length of this region of discontinuity depends on the value of a. We isolated the discontinuity domain by modelling a small stretch of the leading section of the base wall ($0 < \xi \leqslant \varepsilon$) as adiabatic, $(\partial\theta/\partial\eta)_{\eta=0} = 0$. The value of ε was chosen so that it eliminates the numerical instability without affecting quantitatively the solution. The ε value depends on a and the grid fineness: the numerical results described later in this section were obtained using $\varepsilon = 0.02$.

The general trapezoidal domain of the plate fin with inclined crest (Fig. 1, bottom) was mapped onto a unit square, which was covered with a uniform square grid. Finite difference approximations of the transformed governing equations and boundary conditions were applied to the uniform grid. The fineness of the grid was chosen as a trade-off between accuracy and computation time. The accuracy test consisted of comparing the heat generation rate obtained analytically (by integrating equation (13) with equation (17) in the computational domain),

$$\int_{\varepsilon}^{1} \left(\frac{\partial\theta}{\partial\eta}\right)_{\eta=0} \mathrm{d}\xi = \tilde{H}\frac{\varepsilon^{1-a}-1}{1-a^2} \tag{19}$$

with the value of the same integral based on the numerical integration of the temperature solution. A sample of the accuracy test is presented in Table 1: the grid that was chosen for generating the numerical results reported in Sections 3 and 4 was 50×50.

The linear system of finite-difference equations was solved by successive overrelaxation. An optimal overrelaxation coefficient was selected for each case, and the values of this coefficient fell in the range 1.75–1.95. The iteration error was set at 10^{-5}. The numerical results for $\theta(\xi,\eta)$ showed that, as expected, the highest θ value occurs along the base of the fin. We focused then on the base temperature distribution $\theta(\xi,0)$, and identified the temperature and location of the hot spot,

$$\theta_{hot} = \max[\theta(\xi,0)]. \tag{20}$$

A set of representative base temperature distributions is presented in Fig. 2. When the plate thickness is uniform ($a = 0$) the base temperature increases monotonically in the flow direction, and the hot spot is located at the trailing bottom corner of the plate ($\xi = 1, \eta = 0$). As the sharpness parameter a increases, the base temperature becomes more uniform over the downstream 90% of the base length. The hot spot jumps from $\xi = 1$ to a ξ value of order 0.1 as the sharpness parameter exceeds the value $a \cong 0.42$. The hot spot temperature continues to increase as the number a increases above 0.42.

Figure 3 summarizes these observations by showing how θ_{hot} changes as a increases. The filled circles indicate designs in which the hot spot is located at the trailing end of the base. The empty circles correspond to cases where the hot spot is located close to the leading end. It is clear that the sharpness parameter can be selected optimally such that the hot spot temperature is minimized. In Fig. 3, the optimal a value

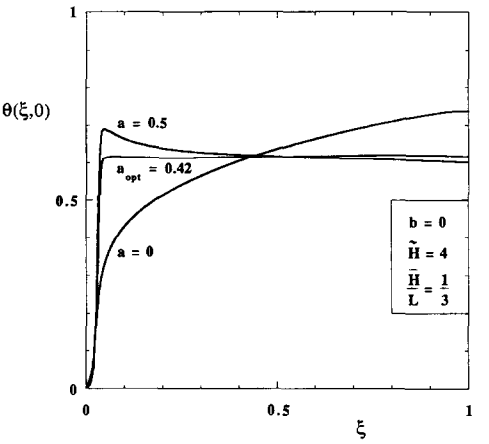

FIG. 2. The effect of the plate sharpness on the temperature distribution along the base of the plate fin.

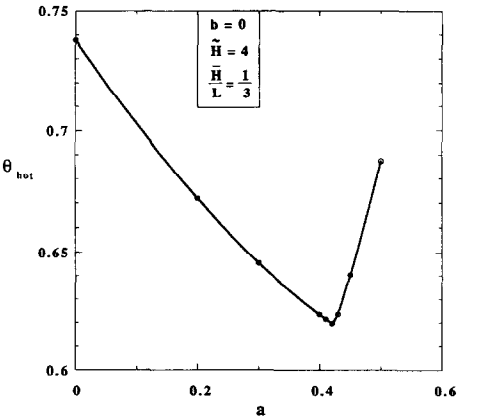

FIG. 3. The effect of the plate sharpness on the temperature difference between the hot spot and the free stream.

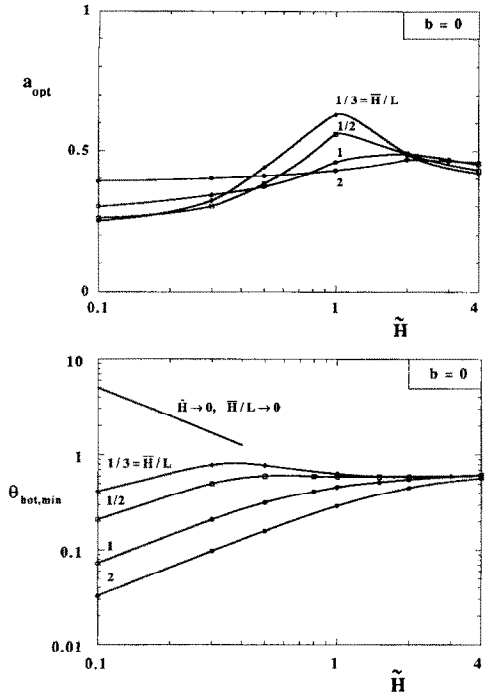

FIG. 4. The optimal sharpness parameter and minimum dimensionless hot spot excess temperature of a plate fin with uniform height.

is close to 0.42, and the hot spot temperature of the plate with uniform thickness ($a = 0$) is 19% greater than the minimum θ_{hot} value that corresponds to $a_{opt} \cong 0.42$. Note further that the optimal design is the one in which the base temperature is the most uniform (Fig. 2). In conclusion, by sharpening the plate in a certain way the designer can (1) minimize the hot spot temperature, and (2) spread almost uniformly the surface temperature of the constant-q'' package.

The optimization process detailed in Figs. 2 and 3 was repeated for many other combinations of $\tilde{H}$ and $\bar{H}/L$, and the conclusions are summarized in Fig. 4. The optimal sharpness parameter a_{opt} takes values of the order of 0.4, and is relatively insensitive to changes in $\tilde{H}$ and $\bar{H}/L$. The minimum hot spot temperature approaches a plateau as $\tilde{H}$ becomes greater than 1, while in the opposite extreme of the $\tilde{H}$ range, it decreases toward 0.

In the limit $\tilde{H} \to 0$ and $\bar{H}/L \to 0$ the fin temperature is mainly a function of x, and not of y. This means that the heat flux released by the lateral $H \times L$ surfaces is uniform ($q'/2\bar{H}$ = constant), and the heat transfer coefficient h_L may be estimated using the boundary layer theory result for a plate with uniform flux (e.g. ref. [8], p. 245). Substituting this h_L estimate in the θ definition (11) we find that at the trailing edge $\theta_{hot} = 1/(2\tilde{H})$, which has been projected on Fig. 4. In conclusion, in the limit $\tilde{H} \to 0$ and $\bar{H}/L \to 0$ the hot spot temperature does not depend on the sharpness parameter a.

4. PLATE WITH VARIABLE HEIGHT AND UNIFORM THICKNESS

The effect of tilting the crest of the fin was considered separately by assuming that the plate thickness distribution is given. For simplicity, the plate thickness was assumed uniform, which is the same as setting $a = 0$ and $\tau = 1$ in the model of Section 2. The tilting of the crest was governed by the dimensionless slope b of equation (7). The b parameter was given only values that fall in the vicinity of $b = 0$, i.e. around the reference design of a fin with uniform height. This

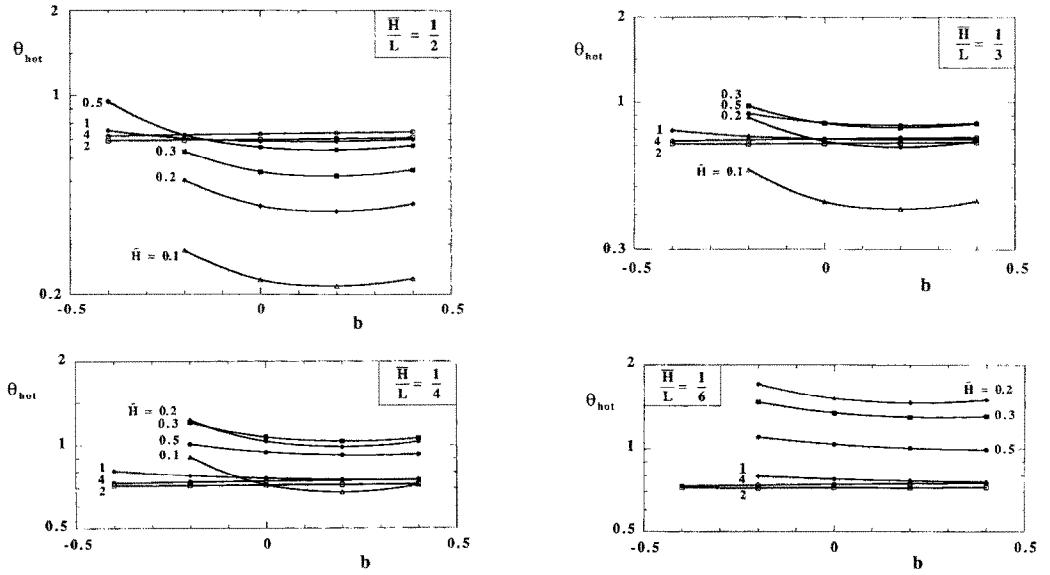

FIG. 5. The effect of the crest inclination on the temperature difference between the hot spot and the free stream ($a = 0$).

limitation on the range of allowable b values is placed by the h model (6), in which it was assumed that the boundary layer starts at $x = 0$ for all y values. The h model breaks down in the vicinity of a tilted crest, and this vicinity would represent a significant portion of the average height $\tilde{H}$ if b were to take values comparable with 1 and -1.

The numerical work proceeded along the path described in the preceding section. Figure 5 shows that the inclination of the crest influences the temperature difference between the hot spot and the free stream. The hot spot is always located at the trailing point of the base. The figure seems to suggest that there exists an optimal slope b_{opt} such that θ_{hot} is minimized, however, we must keep in mind that the present formulation is valid for crests that are tilted only slightly (i.e. for small b). We learn that in the vicinity of $b = 0$ the hot spot temperature decreases as b increases. Note also that the b parameter loses its effect as $\tilde{H}$ increases above 1, because in this limit the crest region is almost as cold as the ambient, and becomes 'inert' in a heat transfer sense.

5. THREE-DIMENSIONAL NUMERICAL MODEL OF THE FIN WITH VARIABLE HEIGHT AND UNIFORM THICKNESS

In the preceding section we used a simple model to show that the fin performance can be improved by

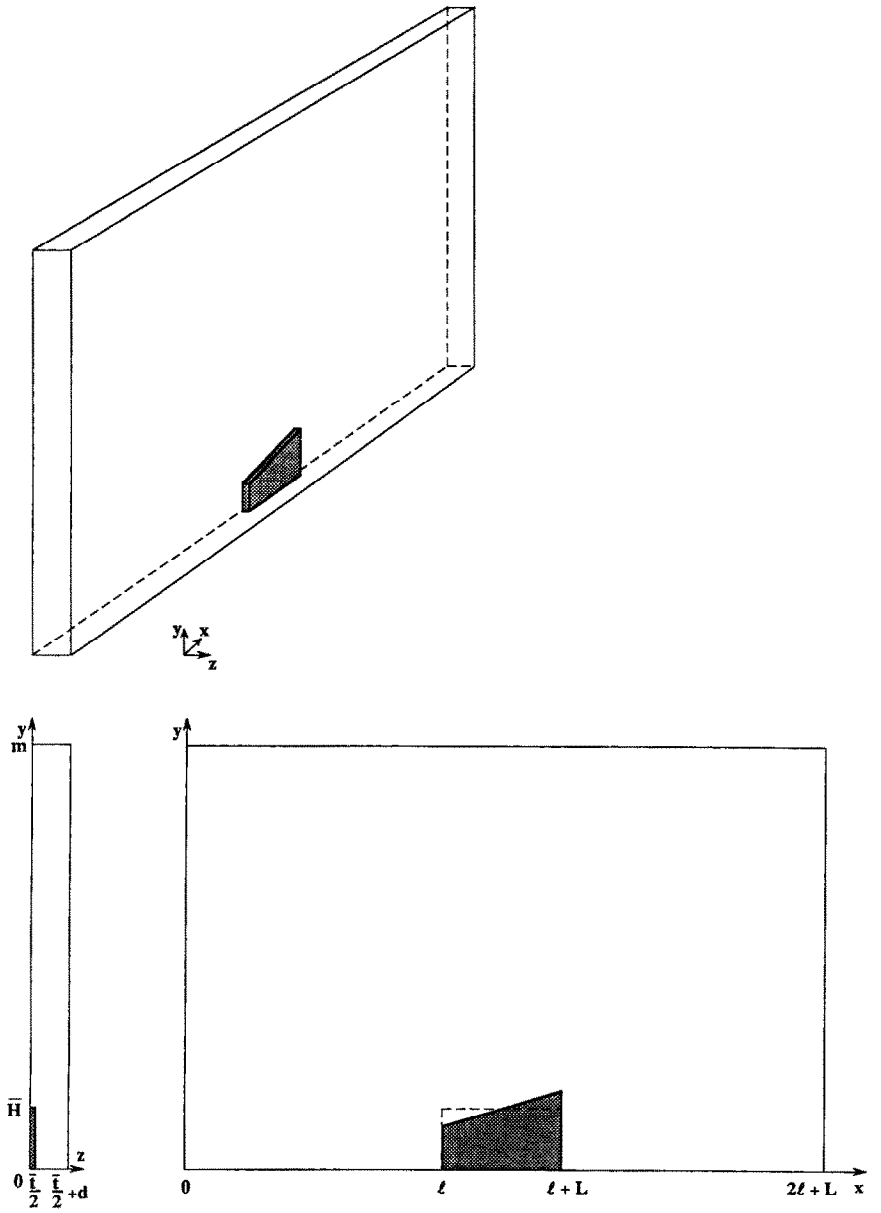

FIG. 6. The computational domain used for three-dimensional simulations of the fin with variable height.

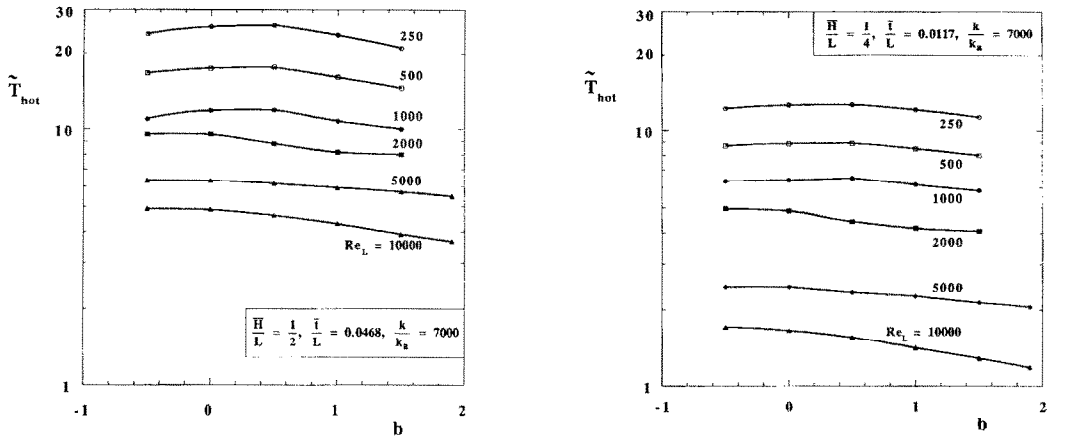

FIG. 7. Three-dimensional numerical results showing the relation between the tilting of the crest and the hot spot temperature.

appropriately tilting its crest. In this section we pursue this conclusion further, with the objective of developing more accurate information for fin design. The new model is based on Fig. 6 and consists of simulating numerically the flow and temperature fields associated with a single fin.

Symmetry allows us to study only one half of the fin and surrounding flow. The computational domain extends from the plane of symmetry of the fin to a parallel plane sufficiently far in the free stream. The chosen distance between these two planes is greater than the thickness of the boundary layer that coats the fin ($LRe_L^{-1/2}$). Numerical tests indicated that this distance (d in Fig. 6) is large enough that it does not

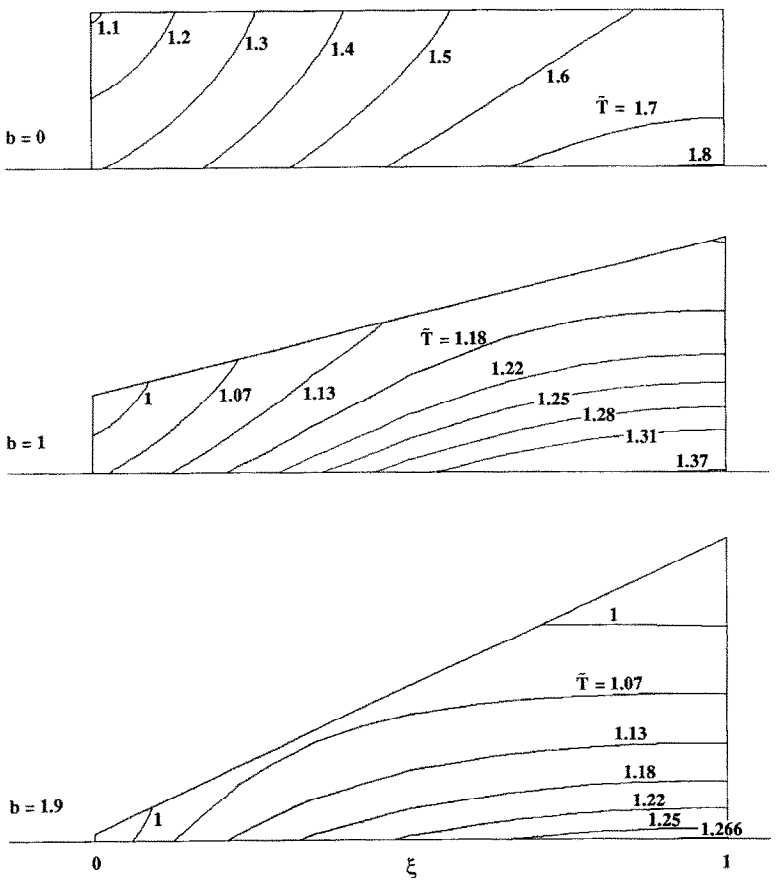

FIG. 8. The isotherms in the plane of symmetry of the plate fin ($Re_L = 10000$, $\bar{H}/L = 1/4$, $\bar{t}/L = 0.0117$, $k/k_a = 7000$; the flow is from left to right).

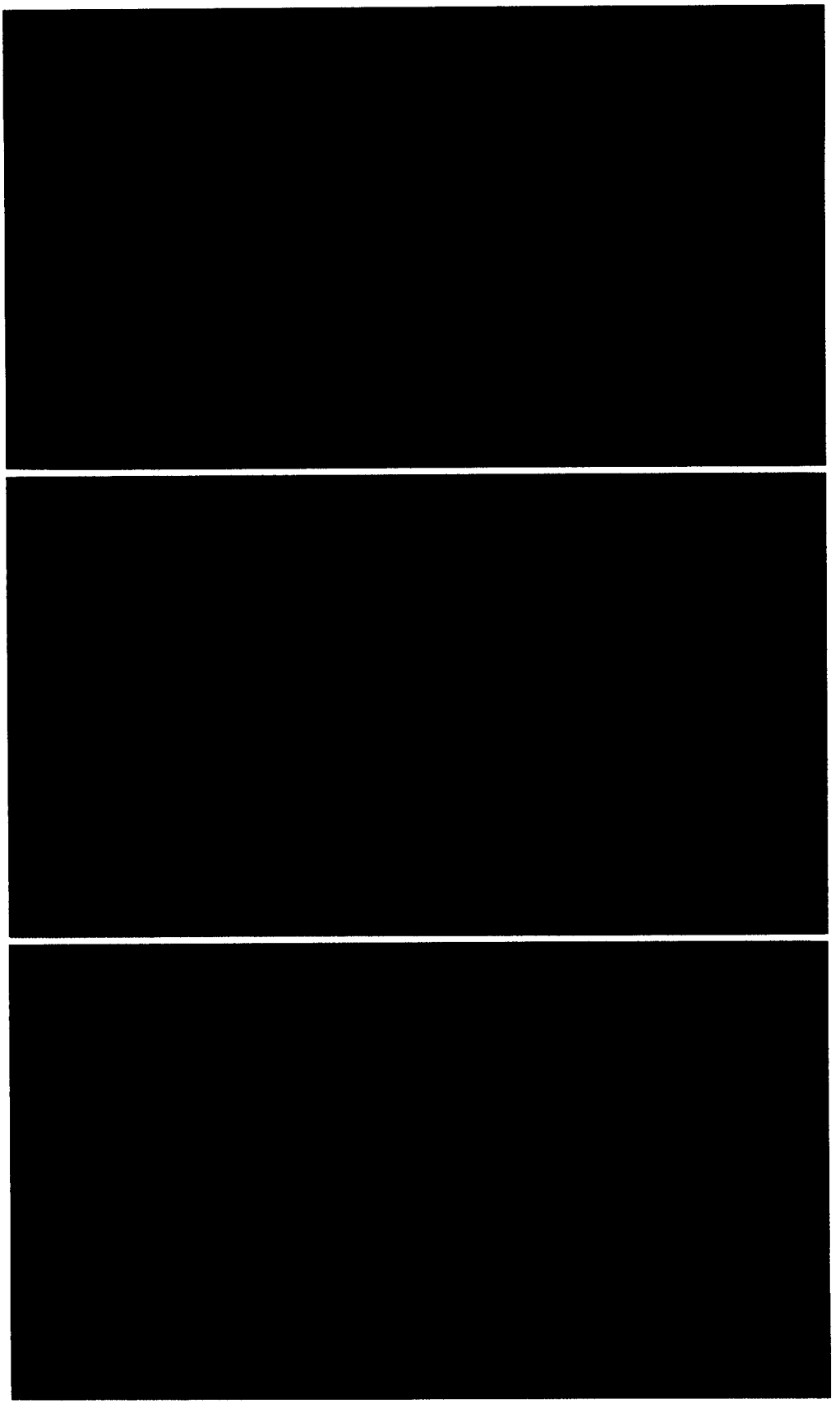

FIG. 9. Color coded isotherms of the case presented in Fig. 8.

influence the results obtained for the fin temperature. Similarly, the domain is sufficiently tall and long (upstream and downstream) to allow the proper simulation of the flow around and over the fin. The chosen length and height of the computational domain are represented by the dimensions $m = 7\bar{H}$ and $l = 2L$, which are defined in Fig. 6.

The nondimensionalized equations that govern the steady laminar flow are

$$\frac{\partial U}{\partial X}+\frac{\partial V}{\partial Y}+\frac{\partial W}{\partial Z}=0 \tag{21}$$

$$U\frac{\partial U}{\partial X}+V\frac{\partial U}{\partial Y}+W\frac{\partial U}{\partial Z}=-\frac{\partial P}{\partial X}+\frac{1}{Re_L}\nabla^2 U \tag{22}$$

$$U\frac{\partial V}{\partial X}+V\frac{\partial V}{\partial Y}+W\frac{\partial V}{\partial Z}=-\frac{\partial P}{\partial Y}+\frac{1}{Re_L}\nabla^2 V \tag{23}$$

$$U\frac{\partial W}{\partial X}+V\frac{\partial W}{\partial Y}+W\frac{\partial W}{\partial Z}=-\frac{\partial P}{\partial Z}+\frac{1}{Re_L}\nabla^2 W, \tag{24}$$

where $\nabla^2 = \partial^2/\partial X^2+\partial^2/\partial Y^2+\partial^2/\partial Z^2$. The dimensionless variables are defined by

$$(X,Y,Z)=\frac{(x,y,z)}{L},\quad (U,V,W)=\frac{(u,v,w)}{U_\infty} \tag{25}$$

$$P=\frac{p}{\rho U_\infty^2},\quad Re_L=\frac{U_\infty L}{\nu}. \tag{26}$$

The energy equations inside and outside the fin are, respectively,

$$\nabla^2\tilde{T}=0 \tag{27}$$

$$U\frac{\partial\tilde{T}}{\partial X}+V\frac{\partial\tilde{T}}{\partial Y}+W\frac{\partial\tilde{T}}{\partial Z}=\frac{1}{Pe_L}\nabla^2\tilde{T}, \tag{28}$$

where

$$\tilde{T}=\frac{T-T_\infty}{q_1/(k\bar{t})},\quad Pe_L=\frac{U_\infty L}{\alpha}. \tag{29}$$

In the denominator of the $\tilde{T}$ definition, q_1 is the heat transfer through the base of the fin. The heat flux through the base is assumed uniform, $q_1/(\bar{t}L)$ = constant. The nondimensionalized boundary conditions that correspond to the domain of Fig. 6 are:

$$\frac{\partial U}{\partial Z}=0,\quad \frac{\partial V}{\partial Z}=0,\quad W=0$$

$$\text{at}\quad Z=0\quad\text{and}\quad Z=\frac{0.5\bar{t}+d}{L} \tag{30}$$

$$V=0\quad\text{at}\quad Y=0\quad\text{and}\quad Y=m/L \tag{31}$$

$$\frac{\partial U}{\partial Y}=0,\quad \frac{\partial W}{\partial Y}=0\quad\text{at}\quad Y=m/L \tag{32}$$

$$U=1,\quad V=0,\quad W=0\quad\text{at}\quad X=0 \tag{33}$$

$$\frac{\partial\tilde{T}}{\partial Y}=-1\quad\text{at}\quad Y=0,\quad 0\leqslant Z\leqslant\frac{\bar{t}/2}{L},$$

$$\frac{l}{L}\leqslant X\leqslant\frac{l}{L}+1 \tag{34}$$

$$\tilde{T}=0\quad\text{at}\quad X=0. \tag{35}$$

In addition to these boundary conditions, we specified that the wetted surfaces of the fin are impermeable and without slip, and that the temperature and heat flux vary continuously across the wetted surfaces. The continuity of heat flux conditions (not listed here) contain the thermal conductivity ratio k/k_a: in all the numerical runs this ratio was set equal to 7000, which is the value for aluminum/air.

The numerical problem (21)–(35) was solved by the finite element method using the code FIDAP [11]. The computational domain was discretized nonuniformly with isoparametric brick elements with eight nodes. The number of elements was chosen such that the solution is grid-independent. The results described in this section were obtained using a mesh with 6180 elements (7595 nodes). The accuracy criteria used were: (1) a relative error of less than 0.1% in the overall pressure drop when the number of grid elements changes by 10%, and (2) a relative error of less than 10% in the stress components on the fin surfaces when the height of the domain changes by 20%. Trilinear interpolation functions were used to approximate the velocity and temperature fields. For the pressure field, we selected the discontinuous penalty approach with a 10^{-6} error factor.

As this is a problem of forced convection, the flow field was determined first, and the temperature field second. The flow solution required roughly 1600–2000 s on the CRAY Y-MP at the North Carolina Supercomputer Center. The convergence criterion was 10^{-3} for both the maximum relative error of the velocity solution and the operator residual vectors. A combined successive substitution/quasi-Newton (Broyden) iterative solution strategy was used to solve the nonlinear algebraic system of equations produced by the Galerkin weighted residual scheme.

Figure 7 shows a summary of all the numerical runs executed using the three-dimensional model. We considered two plate thicknesses ($\bar{t}/L = 0.0468$ and 0.0117), and two average crest heights ($\bar{H}/L = 1/2$ and 1/4). We varied the crest inclination b from -0.5 to 1.9, which is a domain much wider than what we saw in Section 4. The free-stream velocity varied widely, such that the Reynolds number based on the swept length L covered the range 250–10 000. Plotted on the ordinate of Fig. 7 is the dimensionless excess temperature of the hot spot, $\tilde{T}_{hot}$, which is defined by equation (29). The hot spot always occurred on the base, in the plane of symmetry of the plate fin, and very close to the trailing edge.

Several features of Fig. 7 are worth noting. First, the hot spot temperature decreases as b increases only when Re_L is greater than approximately 2000, i.e. when the sides of the fin are lined by distinct (thin) boundary layers. This feature is consistent with the model used in Section 4. The slope of the curve $\tilde{T}_{hot}(b)$ becomes steeper as Re_L increases. The decrease of the hot spot temperature can be significant: for example,

when $Re_L = 10\,000$ in the lower frame of Fig. 7, $\tilde{T}_{hot}$ decreases to 68% of its original value as b increases from 0 to 1.9.

Figure 7 also shows that at Re_L values of order 1000 or less, the tilting of the crest has a relatively small effect on the hot spot temperature. This small effect is such that $\tilde{T}_{hot}$ has a weak maximum with respect to b: the least advantageous inclination (the highest $\tilde{T}_{hot}$) corresponds to b values of approximately 0.5.

The patterns of isotherms of Fig. 8 show why the hot spot temperature decreases as the crest is tilted to 'look' at the approaching air stream. When the height is constant ($b = 0$), the isotherms are inclined at roughly the same angle ($\sim 45°$): this indicates a temperature that increases from left to right along the base, and a portion of the fin (the upper left region) that is relatively cold, i.e. ineffective. The tilting of the crest places more fin material where it is needed the most (near the trailing edge). The isotherms themselves mimick the direction of the crest (Fig. 8, bottom), and this means that the crest temperature is nearly uniform.

In addition to lowering the hot spot temperature, the tilting of the crest spreads the hot spot over a wider region along the base. This is an important feature because it translates into smaller temperature gradients and smaller thermal stresses in the electronic module.

These conclusions are illustrated further in Fig. 9, which is a color display of the temperature fields of Fig. 8. The color code consisted of asignning red to the highest temperature (the bottom-right corner in the top frame) and blue in the free stream (not shown). The proliferation of yellow as the crest becomes more inclined indicates that the fin and the hot spot become colder, and that the fin and its base become more isothermal.

Finally, it is worth nothing that the tilted-crest shapes of Figs. 8 and 9 (the middle and bottom frames) may seem like the plate fins used on the outside of the liquid encapsulated module [3, 12]. In the latter, the crest was inclined in the other direction, i.e. the fin was taller near the start of the boundary layer (air natural convection). That feature was the result of using the variable fin height to compensate for the variation of the heat transfer coefficient on the liquid side of the base wall on which the fins were mounted. The present study makes the point that the heat-sink performance on the air side alone can be improved by tilting the fin crests as shown in the lower part of Figs. 8 and 9.

6. CONCLUSIONS

In this paper we showed that the hot spot temperature of a finned module can be decreased by allowing the plate fin thickness and height to increase in the flow direction. We reached these conclusions by using two models. In the two-dimensional model of Section 2, we uncoupled the fin conduction from the external convection by assuming that the heat transfer coefficient varies as $x^{-1/2}$, in accordance with boundary layer theory. The two-dimensional model breaks down when the inclination of the crest of the fin becomes excessive. In the second part of the paper we solved numerically the three-dimensional problem of conjugate fin conduction and external convection. Here are the main conclusions and ideas for future research.

(1) The maximum temperature on the base of a fin with constant height is reduced by approximately 15% if the plate fin is sharpened like a dull knife such that its thickness increases as $x^{0.42}$, cf. equation (17) and Fig. 3.

(2) The hot spot temperature at the base of a fin with constant thickness is reduced by approximately 30% if the crest is inclined to face the flow, with nearly zero height at the leading edge, as shown in the bottom frames of Figs. 8 and 9. The forward inclination of the crest is the result of having assumed that the base of the fin is heated with uniform flux. It can be shown that when the top of the module is conductive enough that the fin base is isothermal, the optimal crest inclination has a negative b, i.e. the crest looks downstream.

(3) In addition to lowering the hot spot temperature, each of the design changes (1) and (2) leads to a considerably more uniform temperature distribution on the module surface on which the finned heat sink is installed.

(4) It is conceivable that an even greater reduction in hot spot temperature can be achieved by implementing the design features (1) and (2) simultaneously. To determine the actual magnitude of this combined reduction would be a good topic for a future three-dimensional numerical study of the conjugate fin-conduction and convection problem (including conduction inside the module), in which the sharpness and tilting parameters (a, b) both vary.

(5) A simpler way to proceed would be, first, to design the plate fin with constant thickness and height by using the classical method (e.g. ref. [8], pp. 65–67) and, second, to reshape the thickness and height distributions according to conclusions (1) and (2) above, while keeping the fin volume (weight) fixed. To determine how well this simpler approach approximates the optimal design produced numerically by varying a and b, can be the second objective of the future study described at (4) above.

Acknowledgements—This work was conducted during Dr M. Morega's 1992–93 visit to Duke University, and was supported by the IBM Corporation, Research Triangle Park. The guidance received from Dr Sang W. Lee is gratefully appreciated. The numerical work was supported by a grant received from the North Carolina Supercomputing Center.

REFERENCES

1. R. C. Chu, Recent development of computer cooling technology, keynote paper, *6th Int. Symp. on Transport*

Phenomena in Thermal Engng (*ISTP*-6), Seoul, Korea, 9–13 May (1993).
2. G. Taguchi, Robust technology development, *Mech. Engng* **115,** 60–62 (1993).
3. F. P. Incropera, Convection heat transfer in electronic equipment cooling, *J. Heat Transfer* **110,** 1097–1111 (1988).
4. A. D. Kraus, Sixty-five years of extended surface technology (1922–1987), *Appl. Mech. Rev.* **41**(9), 321–364 (1988).
5. A. Aziz, Optimum dimensions of extended surfaces operating in a convective environment, *Appl. Mech. Rev.* **45**(5), 155–173 (1992).
6. W. Nakayama, H. Matsushima and P. Goel, Forced convective heat transfer from arrays of finned packages. In *Cooling Technology for Electronic Equipment* (Edited by W. Aung), pp. 195–210. Hemisphere, New York (1988).
7. A. Bejan and E. Sciubba, The optimal spacing of parallel plates cooled by forced convection, *Int. J. Heat Mass Transfer* **35,** 3259–3264 (1992).
8. A. Bejan, *Heat Transfer*. Wiley, New York (1993).
9. A. Bejan, *Convection Heat Transfer*. Wiley, New York (1984).
10. C. A. J. Fletcher, *Computational Techniques for Fluid Dynamics*, 1, *Fundamental and General Techniques*. Springer, New York (1988).
11. *FIDAP Theoretical Manual*, Fluid Dynamics International, Evanston, IL, V. 6.3 (1991).
12. N. G. Aakalu, R. C. Chu and R. E. Simons, Liquid encapsulated air cooling module, US Patent No. 3, 741, 292 (1973).